Earthquake Engineering & Structural Dynamics

WILEY

RESEARCH ARTICLE OPEN ACCESS

Dual Graph-Based Bayesian Network Modeling With Rao-Blackwellization for Seismic Reliability and Complexity Quantification of Network Connectivity

Dongkyu Lee[1] | Ji-Eun Byun[2] | Junho Song[3]

[1]Engineering Risk Analysis Group, Technical University of Munich, Munich, Germany | [2]James Watt School of Engineering, University of Glasgow, Glasgow, UK | [3]Department of Civil and Environmental Engineering, Seoul National University, Seoul, South Korea

Correspondence: Ji-Eun Byun (ji-eun.byun@glasgow.ac.uk) | Junho Song (junhosong@snu.ac.kr)

Received: 10 December 2024 | **Revised:** 24 February 2025 | **Accepted:** 7 April 2025

Funding: This work is supported by the National Research Foundation of Korea (NRF) grant funded by the Korea government (MSIT) (RS-2021-NR059025). The first author is also supported by the Basic Science Research Program through the NRF grant funded by the Ministry of Education (RS-2024–00408907). The third author is also supported by the Institute of Construction and Environmental Engineering at Seoul National University.

Keywords: adaptive importance sampling | Bayesian network | complexity analysis | connectivity reliability | junction tree algorithm | Rao-Blackwellization

ABSTRACT

Modern societies depend on various lifeline networks such as transportation, electricity, and gas distribution systems, which are vulnerable to seismic events. Although numerous analytical and simulation-based methods have been developed for efficient seismic system reliability analysis (SRA), dealing with high-dimensional events arising from large-scale infrastructure networks remains challenging. To address this challenge, this paper proposes a system reliability method that efficiently computes the connectivity of directed graphs. The method employs the dual graph representation of a target system to automate the construction of a Bayesian network (BN). This enables the application of the junction tree algorithm, a well-established BN inference method, to perform reliability analysis and quantify complexity based on a network topology. The paper further tackles SRA challenges associated with fully correlated seismic uncertainties, which typically lead to a significant increase in computational complexity. To this end, we propose to combine a cross entropy-based adaptive importance sampling technique with Rao-Blackwellization. Thereby, sampling methods and exact analytical inference can be effectively combined to improve computational efficiency for seismic SRA of lifeline networks. The proposed methods are demonstrated through three numerical examples.

1 | Introduction

Lifeline networks that support transportation and services such as electricity, water, and gas are a critical backbone of modern societies. As these network systems become increasingly complex and interconnected, they function as a collective entity rather than a set of independent components. In the face of earthquakes, such interdependence may result in cascading failures, extending beyond the initial physical damage to components. For example, a seismic event may damage lifeline systems, resulting in casualties and economic losses at an extended scale. To mitigate such seismic risks and maximize the efficiency of evacuations, many emergency evacuation plans utilize contraflow lane reversal [1, 2], which requires the accurate vulnerability assessment of lifeline systems and quantification of varying contributions of relevant factors.

Seismic system reliability analysis (SRA) of lifeline *network* systems encounters several computational challenges, including identifying high-dimensional failure domains, managing

exponentially growing combinations, and calculating low system failure probabilities. To address these challenges, various SRA methods handling complex networks have been developed, for example, approximation methods [3], bounds methods [4–6], simulation-based approaches [7–10], and surrogate modeling-based methods [11, 12]. Although these methods represent significant advances in the SRA of large-scale networks, they still face substantial limitations in practical applications. A primary challenge is the difficulty in quantifying the complexity of SRA, including the applicable coverage of the method. Furthermore, especially for simulation-based approaches, their accuracy and efficiency drastically decrease when dealing with low-probability events. In addition, current methods often fail to explicitly exploit the causal dynamics of a system failure event, which hampers the planning of effective mitigation strategies.

Causal relationships can be effectively represented by employing a probabilistic graphical model, *Bayesian network* (BN) [13]. BN's visualization of causal relationships facilitates not only prediction but also diagnostic reasoning—identifying likely causes given observed effects—which is invaluable when pinpointing potential failures is critical. However, they are quickly confronted with computational challenges due to the exponentially increasing computational memory of conditional probability tables (CPTs) as a system size grows. Numerous studies have been proposed to address this issue by developing efficient BN structures for modeling system performance [14], data processing techniques [15], data structures [16, 17], or sampling-based BN inference [18, 19]. Despite these efforts to expand the range of applicable systems, BN-based methods still have limitations in the addressable number of components. In addition, there are no systematic methods for quantifying the precise extent of this limitation (i.e., the number of addressable components), which would provide insightful information for selecting an appropriate SRA method.

This paper proposes a BN-based reliability method for network systems and their complexity quantification. Among many possible definitions of network performance, this paper focuses on the connectivity of an origin-destination (OD) pair in directed graphs. This measure represents, for example, the accessibility to hospitals, healthcare locations, and temporary housing from residential areas in preplanned lane reversal scenarios on highways. That is, the system failure probability is defined as the probability that there are no viable paths for a given OD pair. The focus of this paper is on networks represented by directed acyclic graphs (DAGs), but the proposed preprocessing schemes can address presence of cycles. The construction of BN is automated by the dual graph of a target system. Then, the junction tree (JT) algorithm, a well-established BN inference method, can be applied to the constructed BN to perform SRA and complexity quantification, which depends on the topology of the systems [20]. Building upon this development, we extend the SRA to account for fully correlated random variables that arise from seismic uncertainties. By implementing a cross-entropy-based adaptive importance sampling (CE-AIS) [21–26] for a subset of random variables in a BN and applying the JT algorithm to the remaining variables [17, 27], the proposed method can efficiently combine exact analytical inference and sampling algorithms. Moreover, the method can be readily extended to facilitate probabilistic inference, such as parameter sensitivity analysis. These capabilities enable the proposed framework to provide actionable insights into the seismic resilience of network systems.

The paper is organized as follows. Section 2 briefly reviews BN and JT and introduces the concept of graphical representation, including primal and dual representation of lifeline systems. Section 3 presents a new SRA method based on BN and JT using dual graphs with preliminary works to enhance the usability and efficiency of the method. This section also proposes a method to quantify the complexity of SRA in various topologies. In Section 4, the proposed method integrated with CE-AIS and the Rao-Blackwellization (RB) technique is applied to seismic SRA. Then, in Section 5, three numerical examples are analyzed to demonstrate the efficiency and usefulness of the proposed method. Finally, the conclusions and recommendations for future work are given in Section 6.

2 | Background

2.1 | Probabilistic Graphical Models

2.1.1 | Bayesian Network

A BN is a probabilistic graphical model that visualizes the directional dependence between random variables. A BN can be described as a DAG, $G = (\boldsymbol{N}, \boldsymbol{E})$, where $\boldsymbol{N}$ denotes a set of the nodes corresponding to the random variables, and $\boldsymbol{E}$ is a set of directed edges indicating directional dependencies between pairs of nodes. When an edge points from node N_i to node N_j, they are referred to as a *parent* node and its *child* node, respectively.

Once a BN is constructed, each node $N_i \in \boldsymbol{N}$ has to be quantified through a probability distribution that depends on its parent nodes $Pa(N_i)$, that is, $P(N_i|Pa(N_i))$. Subsequently, the overall joint probability distribution $P(\boldsymbol{N})$, represented by a BN, becomes a product of the conditional probabilities of individual nodes, that is,

$$P(\boldsymbol{N}) = \prod_{N_i \in \boldsymbol{N}} P(N_i|Pa(N_i)). \tag{1}$$

Equation (1) shows how BN factorizes a high-dimensional joint probability distribution $P(\boldsymbol{N})$ into lower-dimensional distributions $P(N_i|Pa(N_i))$. In addition to the visualization of conditional independence, such lower-dimensional representation facilitates constructing probability models based on domain knowledge [27]. Moreover, it can significantly reduce the computer memory demand required to store distributions.

However, BNs have limitations in that, as the number of parent nodes increases, the memory required to store the conditional probability $P(N_i|Pa(N_i))$ grows exponentially. This means that, given too many parent nodes, the construction of BNs becomes infeasible. Additionally, the BN must not have any directed cycles, which limits the class of problems that can be handled by the BN methodology. As proposed in Section 3.1.1, this limitation can be overcome by partitioning the cyclic graph into multiple acyclic subgraphs, thereby making the application of BN more versatile.

2.1.2 | Junction Tree Algorithm

The JT algorithm [28] is a graphical method that provides a structured approach to inferring a BN model. Unlike BN, a JT is an undirected tree-shaped graph whose nodes represent each clique (i.e., a set of clustered random variables) and edges describe the intersection of two adjacent cliques (i.e., a set of common variables between a clique pair). A BN can be easily transformed into a JT, for which several general-purpose algorithms [29] and useful tactics (e.g., moralization, triangulation, tree decomposition, and maximum spanning tree) are available [27]. Once a JT is constructed, probabilistic inference can be performed by passing *messages* (in the form of probability distributions) between the cliques of the tree. This message-passing process is equivalent to distributing and combining local probability information across a JT. After updating the messages of all cliques, one can compute the marginal probability distribution of any random variable by visiting a clique that includes the random variables of interest.

The JT algorithm could provide a systematic approach to probabilistic inference and is one of the most powerful methods for BN inference. However, the JT algorithm has a similar limitation to BN in that the required memory grows exponentially with the number of random variables within a single clique. A clique size can increase rapidly when a large number of nodes in a BN are densely connected (i.e., dependent). Various software programs have been developed to implement the JT algorithm, and this paper utilizes the BRML toolkit developed by Barber [29] to set up BN models and run the JT algorithm.

2.2 | Graphical Representation of Lifeline Systems: Primal and Dual Graphs

Lifeline systems consist of various components that are at risk of failure. Their functionality can be represented by a graph, in which node-type components (e.g., bridges, substations) and line-type components (e.g., roads, pipelines) are modeled as vertices and arcs, respectively. To apply the BN-based method proposed in Section 3, all components at risk of failure must be represented as arcs, which can be readily addressed by graph transformation techniques [30–32]. In this paper, an original graph representing a network system of interest is referred to as a "primal graph".

In a "dual graph" representation, arcs in the primal graph are converted to vertices, and vertex pairs are connected if their corresponding arcs are directly connected in the primal one. This alternative representation can reveal the hidden properties that are not apparent in the primal graph [33]. In this study, we propose using a dual representation to construct the BN for reliability analysis by representing fragile arcs as BN nodes (i.e., random variables), as explained in detail in Section 3. To avoid confusion between BN graphs and graphs of lifeline network systems, components in a system are hereafter referred to as *vertices* and *arcs*, while those of BNs (including JTs) are called *nodes* and *edges*.

3 | Proposed System Reliability Analysis Method

This section proposes a novel SRA method that employs BNs, the JT algorithm, and dual graphs. The advantages of the proposed method are three-fold: (1) the computational complexity of an arbitrary network system can be quantified in terms of the required memory; (2) the proposed method can perform probabilistic inference (e.g., connectivity, parameter sensitivity), whose exact solution was previously considered unattainable; and (3) the proposed processes can be implemented by existing BN algorithms, which are readily available in general-purpose software programs.

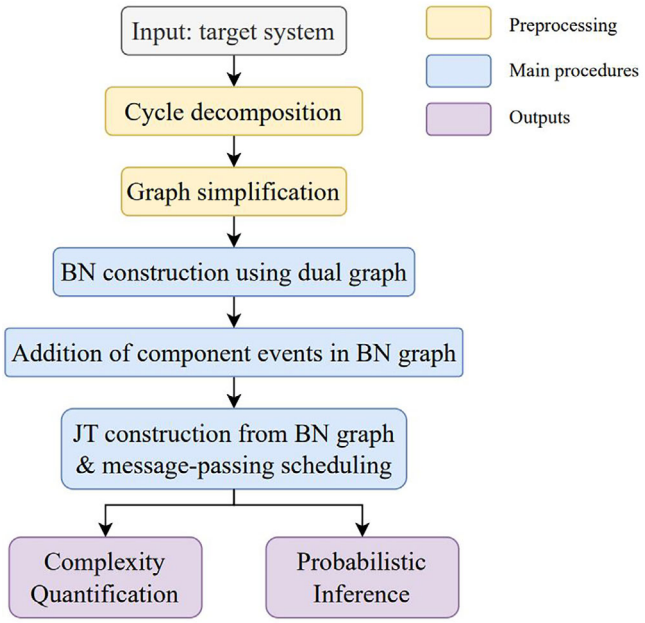

FIGURE 1 | Flowchart of the proposed seismic system reliability analysis (SRA) method.

Before executing the proposed SRA method, two preliminary tasks are conducted to maximize computational efficiency. Then, a BN is automatically constructed by using the dual representation of the preprocessed graph. After adding information about component failure probabilities, one can transform the BN into a JT and obtain a message-passing schedule, which can be done by employing an existing JT algorithm. The final JT model can be used for complexity quantification and probabilistic inference. Figure 1 illustrates an overview of the proposed framework, and the details of each step are described in the following subsections.

3.1 | Preprocessing

3.1.1 | Cycle Decomposition

To mitigate the limitation of BNs in handling graphs with directed cycles, a preprocessing scheme is proposed for decomposing the original cyclic graph into multiple acyclic subgraphs. A cycle is defined as multiple arcs forming a closed polygon, so that the cycle is broken when one or more arcs fail (and thus removed from the graph). If all arcs in a cycle survive, the cycle can be considered as a single super-component. This means that a graph with a single cycle consisting of n arcs can be decomposed into $(n+1)$ directed acyclic subgraphs. Specifically, the first subgraph represents the graph where one arc of the cycle fails, and the second represents the one where the first arc works but another

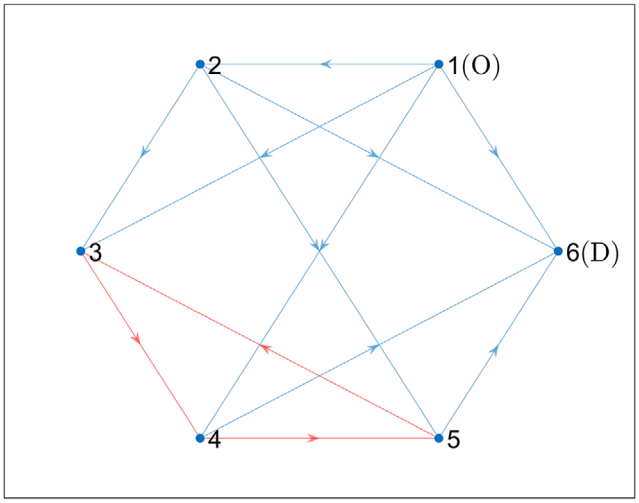

FIGURE 2 | An example directed graph G with a triangular cycle nodes $3 \rightarrow 4 \rightarrow 5$.

arc fails. In this way, the ith subgraph, $i = 1, \ldots, n$, is created with $(i-1)$ arcs in operation and the ith arc broken. Finally, the $(n+1)$th subgraph with all working arcs is equivalent to a graph where the inflow and outflow arcs to the cycle are concentrated on a single super-component (i.e., conceptual vertex) that replaces the whole cycle. The reliability analysis for the graph with n_{cyc} cycles requires n_{sub} decomposed subgraphs with

$$n_{\text{sub}} = \prod_{i=1}^{n_{\text{cyc}}} (n_i + 1) \ , \tag{2}$$

where n_i is the number of arcs in the ith cycle, $i = 1, \ldots, n_{\text{cyc}}$.

For example, consider a random directed graph G with a cycle consisting of three arcs (i.e., $n_{\text{cyc}} = 1$ and $n_1 = 3$) in Figure 2. The origin (O) and destination (D) vertices are set to Vertices 1 and 6, respectively. Then, the cycle decomposition scheme generates $(3+1) = 4$ acyclic subgraphs, $G^1, \ldots, G^4$, as shown in Figure 3. After the decomposition, the failure probability of G in terms of the OD connectivity, $P_f(G)$, can be evaluated based on the failure probabilities of its subgraphs, that is,

$$P_f\ (G) = \sum_{j=1}^{n_{\text{sub}}} L_j P_f\left(G^j\right) \ , \tag{3}$$

where G^j denotes the jth subgraph; L_j is the probability of G^j; and $P_f(G^j)$ is the failure probability of G^j.

This preprocessing technique enables BN-based approaches to handle even undirected graphs that can be decomposed into a set of DAGs. Each undirected arc is equivalent to a cycle with two arcs pointing toward each other. However, analyzing all subgraphs becomes impractical when the number of arcs is large, due to the exponential growth of n_{sub}. In such cases, the top subgraphs with the highest L_j can be selected in a way that their cumulative probability sum, $\sum L_j$, reaches a target threshold (e.g., $L^t = 0.95$). This approach allows for the computation of upper and lower bounds, with a width of $1 - \sum L_j$ [6]. Previous research such as [6, 34] has shown that a significantly small subset of subgraphs often accounts for a probability close to one.

3.1.2 | Graph Simplification

When dealing with large-scale directed graphs, a large fraction of vertices may be unreachable from Vertex O or to Vertex D, making SRA unnecessarily complex. To further simplify SRA, we propose the second preprocessing strategy that removes these vertices, and the arcs connected thereto in the primal graph or its subgraphs. This strategy can be implemented by any basic connectivity analysis algorithms, including minimum spanning tree. Since these are highly dependent on an OD pair, the need for each component may vary depending on the OD vertices, even within the same graph.

This optional preprocessing step is highly recommended, especially for large-scale graphs. Marginalization can eliminate unnecessary random variables during message passing in a JT. With the proposed preprocess, however, the computation becomes much more efficient than the procedure with marginalization alone. From numerical experiments, we found that this strategy greatly improves the efficiency of the proposed algorithm. This works particularly well for random graphs, which frequently contain numerous isolated components from the OD pair, providing clues to problems that may be intractable in their original form.

3.2 | Main Procedures

3.2.1 | Automation of BN Construction Using Dual Graph

The proposed method starts by constructing a BN with nodes S and T_i for $i \in [1, N]$, where N represents the number of arcs in the primal graph of a target system. S, representing the system connectivity event, is denoted as a binary random variable, whose value is 1 if the OD pair is connected, and 0 otherwise. Similarly, each T_i is a binary random variable equal to 1 if the head of arc i is reachable from Vertex O, and 0 otherwise. In the BN, node S is located at the position of Vertex D, and nodes T_i are positioned on their respective arcs. Then, the nodes are connected by directed edges to describe the connectivity between arcs in the primal graph. The generated BN has a topology equivalent to the dual representation of the target system, except for S and the edge(s) toward it. In other words, by adding S and its incoming edge(s) to the dual representation of the target system expressed as a DAG, we can automate the construction of the BN.

For example, consider the example network in Figure 4 [35], which has four vertices (blue circles) and five directed arcs (green arrows). Then, an initial BN can be constructed by using the dual representation as shown in the red dashed box in Figure 5. The BN construction is completed by adding node S and two directed edges headed to S (blue circle and arrows in Figure 5).

The proposed method achieves efficiency by leveraging a distinctive characteristics of connectivity analysis that conditional independence holds between arcs that are not directly connected.

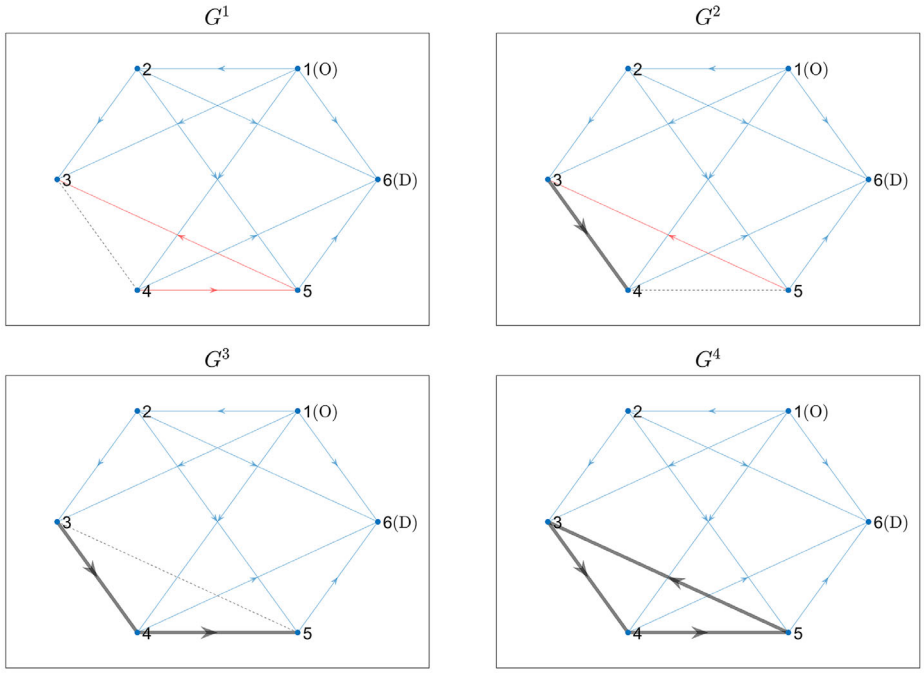

FIGURE 3 | Equivalent subgraphs after cycle decomposition (dashed: failed arcs, black solid: survival arcs, red: unknown).

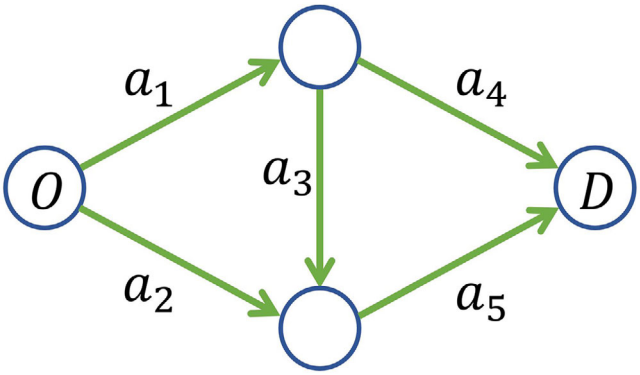

FIGURE 4 | Example graph with five arcs [35].

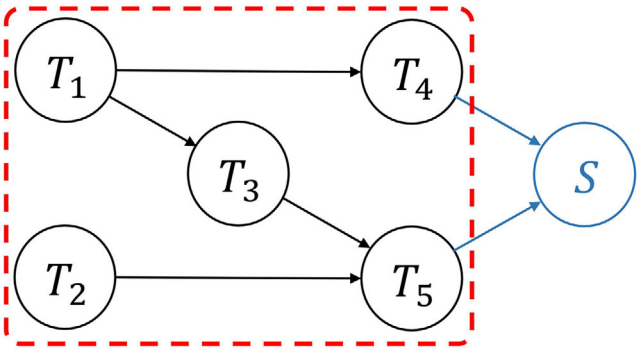

FIGURE 5 | Constructed Bayesian network (BN) via dual representation of the original graph in Figure 4.

In other words, the connectivity of an arc from an origin vertex is independent of the status of the other vertices if the status of the incoming arcs is known. For instance, in Figure 4, the connectivity between Arc 5 and Vertex O is independent of Arcs 1 and 4, conditioned on the connectivity of Arcs 2 and 3. Figure 5 visualizes such independence relationships more intuitively. We note that this characteristic does not hold for other types of analysis, including maximum flow analysis. For example, in a traffic simulation analysis, traffic is assigned sequentially by taking into account traffic flows on both preceding and succeeding arcs.

TABLE 1 | CPT of T_i given X_i.

$P(T_i \mid X_i)$	$T_i = 1$	$T_i = 0$
$X_i = 1$	1	0
$X_i = 0$	0	1

3.2.2 | Addition of Component Failure Events

The BN constructed in Section 3.2.1 contains only topological information of a target system, without considering the component failure events. Therefore, to represent component failure events, binary random variables X_i for $i \in [1, N]$ are introduced, indicating whether arc i is functional ($X_i = 1$) or not ($X_i = 0$). For each i, node X_i is added as a parent node of T_i. If the component failure events are statistically independent, this approach leads to a complete construction of a BN model. For example, Figure 6a illustrates the final BN representing the example graph after adding independent component failure events. The CPT of T_i can be constructed as Table 1 if the Arc i is connected to Vertex O (e.g., Arcs 1 and 2 in Figure 4). On the other hand, if Arc i is reachable from Vertex O but is not connected, the CPT is modified as Table 2. Finally, the CPT of S is presented in Table 3.

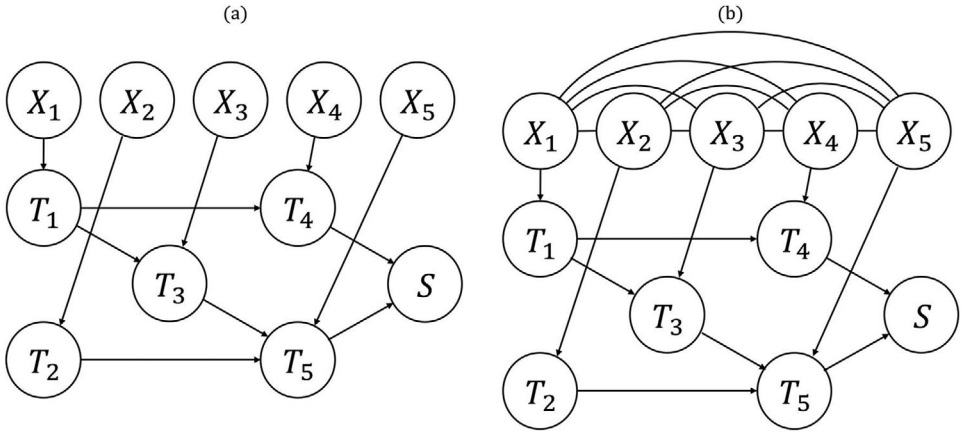

FIGURE 6 | Constructed Bayesian network (BN) of example graph with (a) independent; and (b) interdependent component failure events.

TABLE 2 | CPT of T_i given X_i and $\forall T_k \in Pa(T_i)$.

$P(T_i \mid X_i, \forall T_k \in Pa(T_i))$	$T_i = 1$	$T_i = 0$
$\sum_{T_k \in Pa(T_i)} T_k X_i \geq 1$	1	0
$\sum_{T_k \in Pa(T_i)} T_k = 0$	0	1
$X_i = 0$	0	1

TABLE 3 | CPT of S given $\forall T_k \in Pa(S)$.

$P(S \mid \forall T_k \in Pa(S))$	$S = 1$	$S = 0$
$\sum_{T_k \in Pa(S)} T_k \geq 1$	1	0
$\sum_{T_k \in Pa(S)} T_k = 0$	0	1

If component failure events are interdependent, their dependence needs to be incorporated in the BN graph. For example, Figure 6b shows the modified BN for example graph, where all X_i are correlated and therefore are fully connected by undirected edges.

3.2.3 | JT Construction With Message-Passing Scheduling

For probabilistic inference and complexity quantification, the BN graph constructed in Section 3.2.2 is used to build a JT. This can be done automatically using existing algorithms, including the maximum spanning tree algorithm [29]. Various JTs can be constructed from a single BN depending on the order of clique considerations and triangulations [36]. We note that any JT algorithm is applicable to the proposed method below.

Figure 7a represents an example of the JT corresponding to the BN in Figure 6a. Using the JT graph, the CPTs associated with a clique can be inferred, for example, Table 1 for C_1 and C_2, Table 2 for C_3 to C_5, Table 3 for C_8. For the exact inference of S, the message-passing can be scheduled as $C_1 \rightarrow C_3$, $C_2 \rightarrow C_4$, $C_3 \rightarrow C_6$, $C_4 \rightarrow C_7$, $C_5 \rightarrow C_6$, $C_6 \rightarrow C_7$, and $C_7 \rightarrow C_8$, as shown in Figure 7a. On the other hand, if the component failure events are interdependent as in Figure 6b, the corresponding JT is obtained as shown in Figure 7b. In this case, the message-passing scheme between the two cliques is obtained as $C_1 \rightarrow C_2$. We note that the large clique C_1, containing all component events and arc events, indicates the exponential increase in computational cost. In other words, the interdependency between component failure events makes SRA problems infeasible to solve even with a moderate number of random variables (e.g., 25). We address this issue by the proposed SRA method described in Section 4.

3.3 | Applications of the Proposed Method

3.3.1 | Complexity Quantification of SRA

Since configuring cliques (i.e., multiplying associated CPTs in each clique and storing them) is the bottleneck of computational time and memory, computational complexity can be approximately quantified by the sum of clique sizes (i.e., the number of probabilities in an associated CPT). Since all T_i and X_i are binary random variables, the computational complexity, COL, is defined as

$$COL = \sum_j 2^{n_{\mathrm{cq}_j}}, \tag{4}$$

where n_{cq_j} is the number of random variables in the jth clique. For example, the computational complexity of Figure 7a,b is calculated as $COL_a = 2 \cdot 2^2 + 5 \cdot 2^3 + 2^4 = 64$ and $COL_b = 2^{10} + 2^3 = 1,032$, respectively. The complexity measure can quantify the significantly increased computational cost of the model in Figure 7b.

To investigate the computational complexity measure in Equation (4), four representative graph topologies in Figure 8 are analyzed, assuming statistical independence between component events. Figure 9a,b respectively shows the changes in COL and the maximum clique size for each graph topology as the number of arcs varies from 4 to 150. Interestingly, the logarithm of COL and the maximum clique size exhibit a linear relationship ($R^2 = 99.43\%$ for the entire data in Figure 9). This implies that the largest clique often dominates computational complexity. In line and tree graphs, for example, both the maximum clique size

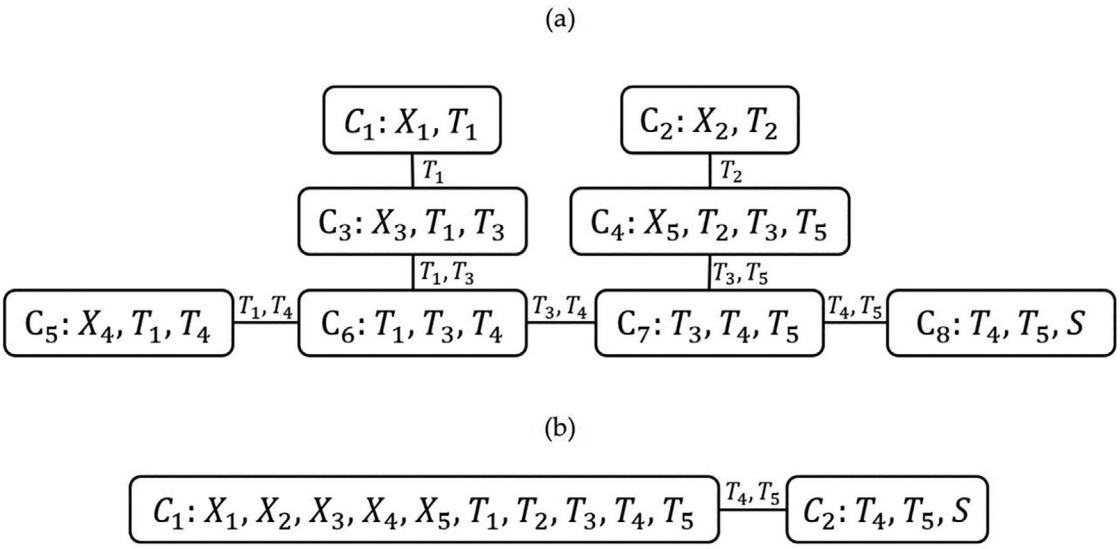

FIGURE 7 | Constructed junction tree (JT) with (a) independent component failure events; and (b) dependent component failure events.

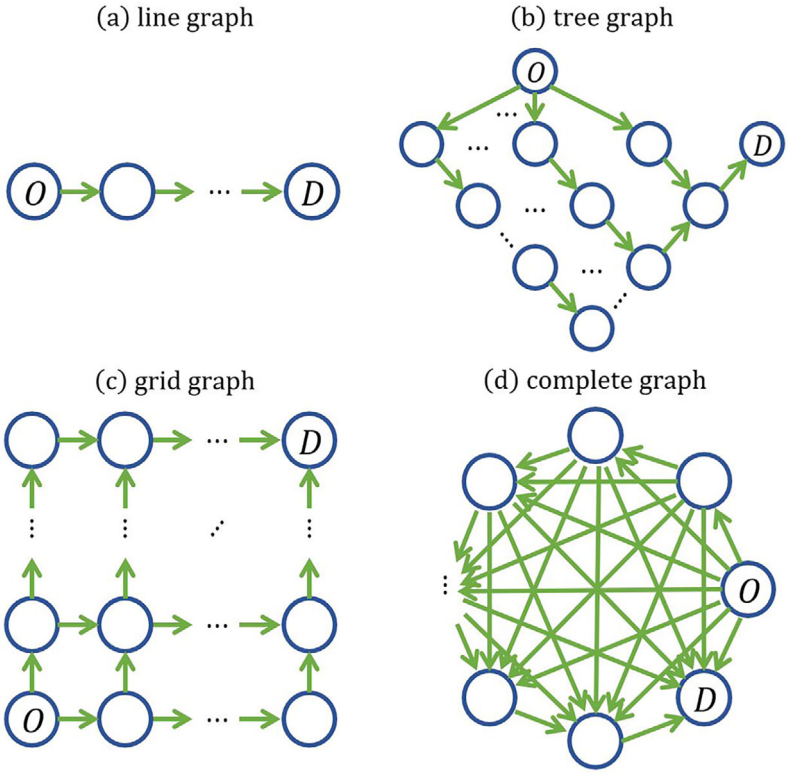

FIGURE 8 | Representative graph topologies.

and *COL* indicate that complexity is almost constant regardless of the number of arcs. On the other hand, in complete graphs, the maximum clique size increases linearly in terms of the number of arcs, which is consistent with the results indicating that *COL* increases exponentially. The maximum clique size of the grid graph also increases with the number of arcs, but at a much slower rate than that of the complete graph. Considering their high proximity, the complexity of the example graphs in Section 4 is measured in terms of maximum clique size instead of *COL*.

The proposed quantification is advantageous as the quantification of graph topology complexity has remained elusive. Although there are several metrics developed to this end [30, 37], the proposed approach provides a direct metric for SRA. Thereby, one can select an appropriate SRA method before performing analysis. If a given topology is found to have too high complexity to apply analytical methods, simulation-based methods or advanced BN inference algorithms can be employed instead of basic BN inference algorithms (e.g., message-passing or variable elimination).

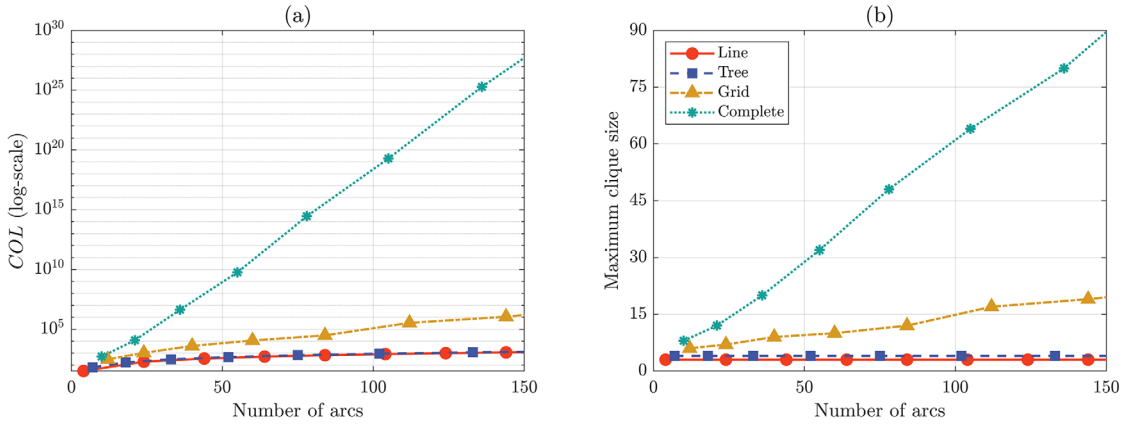

FIGURE 9 | Computational complexity by the number of arcs in each graph topology evaluated in terms of (a) *COL*; and (b) maximum clique size.

3.3.2 | Probabilistic Inference: Analysis of System Reliability and Parameter Sensitivity

If complexity is quantified to be manageable (e.g., all cliques include less than or equal to 25 random variables), an exact system failure probability, $P_f := P(S = 0)$, can be evaluated by performing message-passing of a constructed JT. Manageable complexity is expected when component events are independent, and each vertex in a primal graph has only a few incoming arcs (e.g., Figure 8a–c).

If complexity seems unmanageable, advanced inference strategies, such as RB (also known as collapsed particles) [17, 27], can be employed. RB is regarded as a hybrid approach that generates samples for a subset of random variables while, for other variables, performing exact inference over conditional probability distributions. By strategically selecting the variables to be sampled, exact inference can have significantly lower computational complexity, while effectively controlling a sampling variance.

A JT can also be used to calculate parameter sensitivities of P_f, which provides information on the impact of sudden external actions, such as degradation or reinforcement of components, on the system reliability. The sensitivities of conditional probabilities of component events, $P(N_j|Pa(N_j))$, with respect to a parameter θ_k (e.g., a parameter of seismic capacity) are derived from Equation (1) as

$$\frac{\partial P(\boldsymbol{N})}{\partial \theta_k} = \sum_{N_j \in \boldsymbol{N}} \left[\frac{\partial}{\partial \theta_k} P\left(N_j | Pa\left(N_j\right)\right) \cdot \prod_{N_i \in \boldsymbol{N} - \{N_j\}} P\left(N_i | Pa\left(N_i\right)\right) \right], \tag{5}$$

where each square bracket is computed by replacing the CPT of $P(N_j|Pa(N_j))$ with $\partial P(N_j|Pa(N_j))\ /\partial\theta_k$ in a JT graph [38]. However, even without the CPT of $\partial P(N_j|Pa(N_j))\ /\partial\theta_k$, one can approximate the sensitivity of the system failure probability, $\partial P_f/\partial\theta_k$, via the same message-passing procedure that was previously scheduled as

$$\frac{\partial P_f}{\partial \theta_k} \cong \frac{P\left(S = 0 |\ \theta_k = \theta_k^0 + \delta\right) - P_f}{\delta}, \tag{6}$$

where θ_k^0 denotes the initial value of θ_k; and δ denotes a sufficiently small positive constant. A sensitivity measure can be used to evaluate the upgrade worth, which quantifies the impact of each component's reinforcement on the system [39, 40], that is,

$$I_{\theta_k} = -\left[\frac{\partial P_f}{\partial \theta_k}\right] \Delta\theta_k, \tag{7}$$

where I_{θ_k} denotes the upgrade worth of θ_k; and $\Delta\theta_k$ denotes the variation in θ_k that can be achieved by a unit cost increment.

4 | Seismic SRA Using Rao-Blackwellization

4.1 | Seismic SRA of Lifeline Systems

For a seismic SRA, the binary random variable X_i can be defined as an event that the seismic demand of the ith component, D_i exceeds its seismic capacity C_i, that is,

$$X_i = \mathbb{I}\left(C_i \le D_i\right) = \mathbb{I}\left(z_i \le 0\right), \tag{8}$$

where $\mathbb{I}(\cdot)$ denotes a binary indicator function that returns 1 if a given equation/inequality holds, and 0 otherwise; and $z_i := \ln C_i - \ln D_i$ denotes the logarithmic safety margin [41]. We assume that D_i and C_i are statistically independent of each other. To quantify the intensity of earthquakes, various ground-motion parameters, e.g., peak ground acceleration (PGA), peak ground velocity (PGV), pseudo-spectral acceleration (PSA), can be used [42–44]. In this paper, both D_i and C_i are quantified by PGA values.

The seismic demand D_i can be predicted by a ground motion prediction equation [45, 46] such as

$$\ln D_i = f\left(M, R_i, \boldsymbol{\lambda}_i\right) + \eta + \varepsilon_i, \tag{9}$$

where $f(\cdot)$ represents the attenuation relation of PGA, which depends on the earthquake magnitude M, the distance R_i from the epicenter to the site i, and a set of other explanatory variables $\boldsymbol{\lambda}_i$; η is the interevent residual with a zero mean and a standard deviation of σ_η; and ε_i is the intraevent residual with a zero mean and a standard deviation of σ_ε. Although η accounts for

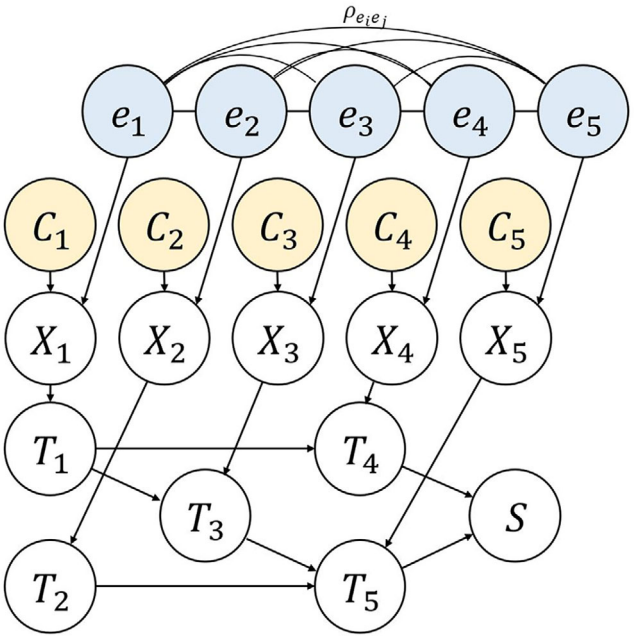

FIGURE 10 | Bayesian network (BN) for seismic reliability analysis of the example graph in Figure 6b.

the common randomness of seismic demand occurring within an earthquake due to its inherent seismic properties, ε_i captures the remaining randomness, which is mainly distributed spatially [47]. Although η and ε_i are assumed to be statistically independent of each other, the spatial correlation between ε_i and ε_j, $\rho_{\varepsilon_i\varepsilon_j}$, is given as a function of the distance Δ_{ij} between sites i and j. By introducing the total residual $e_i := \eta + \varepsilon_i$ with a zero mean and a standard deviation of $\sigma_{e_i} = \sqrt{\sigma_\eta^2 + \sigma_\varepsilon^2}$, one can derive the correlation coefficient between $\ln D_i$ and $\ln D_j$, $\rho_{\ln D_i \ln D_j}$, as

$$\rho_{\ln D_i \ln D_j} = \rho_{e_i e_j} = \frac{\mathrm{Cov}\left[e_i, e_j\right]}{\sigma_{e_i}\sigma_{e_j}} = \frac{\sigma_\eta^2 + \rho_{\varepsilon_i\varepsilon_j}\left(\Delta_{ij}\right)\sigma_\varepsilon^2}{\sigma_\eta^2 + \sigma_\varepsilon^2}. \tag{10}$$

On the other hand, the seismic capacity C_i is modeled by a lognormal distribution with a median of $\bar{C}_i$ and a lognormal standard deviation of ζ_i. Since each seismic capacity is determined by the structural parameters (e.g., span length, column type) or modeling parameters (e.g., material properties) [48], we can assume that seismic capacities are statistically independent of each other. The GMPE can be incorporated into the proposed BN in Section 3.2.2, introducing random variables C_i and e_i, which respectively represent the capacity and residual of demand of an Arc i. For example, the BN graph in Figure 6b can be extended as illustrated in Figure 10.

4.2 | Rao-Blackwellized Cross-Entropy-Based Adaptive Importance Sampling

4.2.1 | Rao-Blackwellization Technique for Seismic SRA

A vector of the correlated total residuals $\boldsymbol{e} = \{e_1, \cdots, e_N\}$ (blue nodes in Figure 10) is the main cause of large cliques in the JT for a seismic SRA problem. When $\boldsymbol{e}$ is sampled and thereby conditioned in a BN graph, component events become conditionally independent of each other, that is, $(X_i \perp X_j | e_i, e_j)$ for $i \neq j$. It is noted that the BN and JT are identical to those with independent component failure events, except the probabilities of X_i depending on e_i. Consequently, RB can make the seismic SRA problems tractable in terms of COL by iteratively sampling $\boldsymbol{e}$ and evaluating the conditional system failure probability $P(S = 0|\boldsymbol{e})$ using the JT constructed in Section 3 as

$$P_f = E_{p(\boldsymbol{e})}\left[P\left(S = 0|\boldsymbol{e}\right)\right] \cong \frac{1}{n_s}\sum_{k=1}^{n_s} P\left(S = 0|\boldsymbol{e}_k\right), \tag{11}$$

where $E_{p(\boldsymbol{e})}[\cdot]$ denotes the expectation with respect to the joint probability density function (PDF) of $\boldsymbol{e}$, $p(\boldsymbol{e})$; n_s is the number of sampled residual vectors; and $\boldsymbol{e}_k$ is the kth sample vector generated from $p(\boldsymbol{e})$.

However, despite the reduced computational complexity, there are still difficulties in applying RB to a realistic seismic SRA. Especially in large-scale systems, the method requires too many samples as the residuals in $\boldsymbol{e}$ are distributed in a high-dimensional space. Even though message-passing in a JT can be performed rapidly, the required number of samples overwhelms the efficiency in this case. Therefore, standard MCS with full particles, that is, sampling all random variables and identifying the connectivity of sampled systems, can be more efficient than the proposed hybrid method [27]. To complement the sample inefficiency, in the following sections, we adopt CE-AIS [21–26].

4.2.2 | Review: Cross-Entropy-Based Adaptive Importance Sampling

For importance sampling (IS), the original PDF $p(\boldsymbol{e})$ can be replaced by an alternative sampling density function with a parameter vector $\boldsymbol{v}$, $h(\boldsymbol{e}; \boldsymbol{v})$. Then, the estimated P_f is evaluated as

$$\begin{aligned} P_f &= \int \left[\frac{P\left(S = 0|\boldsymbol{e}\right)p\left(\boldsymbol{e}\right)}{h\left(\boldsymbol{e};\boldsymbol{v}\right)}\right] h\left(\boldsymbol{e};\boldsymbol{v}\right) d\boldsymbol{e} \\ &= \int \left[P\left(S = 0|\boldsymbol{e}\right) W\left(\boldsymbol{e};\boldsymbol{v}\right)\right] h\left(\boldsymbol{e};\boldsymbol{v}\right) d\boldsymbol{e} \\ &\cong \frac{1}{n_s}\sum_{j=1}^{n_s} P\left(S = 0|\boldsymbol{e}_j\right) W\left(\boldsymbol{e}_j;\boldsymbol{v}\right), \end{aligned} \tag{12}$$

where $W(\boldsymbol{e}; \boldsymbol{v}) = p(\boldsymbol{e})/h(\boldsymbol{e}; \boldsymbol{v})$ is the likelihood ratio of the original PDF to the alternative sampling PDF; and $\boldsymbol{e}_j$ is the jth sample vector generated from $h(\boldsymbol{e}; \boldsymbol{v})$. We note that, in the equation, a typical binary limit-state function is replaced by $P(S = 0|\boldsymbol{e})$ to facilitate RB applications. The variance of the estimate in Equation (12) highly relies on $h(\boldsymbol{e}; \boldsymbol{v})$, whose optimal form $p^*(\boldsymbol{e})$ minimizing the sampling variance is given as [49]

$$p^*\left(\boldsymbol{e}\right) = \frac{\left|P\left(S = 0|\boldsymbol{e}\right)\right| p\left(\boldsymbol{e}\right)}{\int \left|P\left(S = 0|\boldsymbol{e}\right)\right| p\left(\boldsymbol{e}\right) d\boldsymbol{e}} = \frac{P\left(S = 0|\boldsymbol{e}\right) p\left(\boldsymbol{e}\right)}{P_f}. \tag{13}$$

Although the exact solution of Equation (13) cannot be obtained in practice because of the unknown denominator P_f, one can obtain a near-optimal IS density by minimizing the difference between two PDFs, $p^*(\boldsymbol{e})$ and $h(\boldsymbol{e}; \boldsymbol{v})$. Such difference can be

quantified, for example, by the Kullback–Leibler (KL) divergence (also called relative cross-entropy [50]), which is defined as

$$D_{\mathrm{KL}}\left(p^{*} \parallel h\right)=\int p^{*}(\boldsymbol{e}) \ln p^{*}(\boldsymbol{e}) d \boldsymbol{e}-\int p^{*}(\boldsymbol{e}) \ln h(\boldsymbol{e} ; \boldsymbol{v}) d \boldsymbol{e}. \tag{14}$$

In CE-AIS, a near-optimal IS density $h(\boldsymbol{e};\boldsymbol{v})$ is obtained by finding the parameter vector $\boldsymbol{v}$ that minimizes $D_{\mathrm{KL}}(p^{*} \parallel h)$. As the first term of Equation (14) is invariant to $\boldsymbol{v}$, this is equivalent to maximizing the second term only. According to Equation (13), the parameter vector $\boldsymbol{v}$ of a near-optimal IS density is obtained as

$$\begin{aligned}\boldsymbol{v} &= \underset{\boldsymbol{v}'}{\operatorname{argmin}} D_{\mathrm{KL}}\left(p^{*} \parallel h\right) \\ &= \underset{\boldsymbol{v}'}{\operatorname{argmax}} \int p^{*}(\boldsymbol{e}) \ln h\left(\boldsymbol{e} ; \boldsymbol{v}'\right) d \boldsymbol{e} \\ &= \underset{\boldsymbol{v}'}{\operatorname{argmax}} \int P(S=0 | \boldsymbol{e}) \ln h\left(\boldsymbol{e} ; \boldsymbol{v}'\right) p(\boldsymbol{e}) d \boldsymbol{e}\,. \end{aligned} \tag{15}$$

In order to evaluate Equation (15) more efficiently, the parameter vector $\boldsymbol{w}$ of another alternative IS density is introduced as

$$\begin{aligned}\boldsymbol{v} &= \underset{\boldsymbol{v}'}{\operatorname{argmax}} \int\left[\frac{P(S=0 | \boldsymbol{e}) \ln h\left(\boldsymbol{e} ; \boldsymbol{v}'\right) p(\boldsymbol{e})}{h(\boldsymbol{e} ; \boldsymbol{w})}\right] h(\boldsymbol{e} ; \boldsymbol{w}) d \boldsymbol{e} \\ &\cong \underset{\boldsymbol{v}'}{\operatorname{argmax}} \sum_{j=1}^{n_s} P\left(S=0 | \boldsymbol{e}_j\right) \ln h\left(\boldsymbol{e}_j ; \boldsymbol{v}'\right) W\left(\boldsymbol{e}_j ; \boldsymbol{w}\right), \end{aligned} \tag{16}$$

where $\boldsymbol{e}_j$ is the jth sampled residual vector generated from $h(\boldsymbol{e};\boldsymbol{w})$. In CE-AIS, $\boldsymbol{w}$ is generally set to the value of $\boldsymbol{v}$ updated in the previous iteration [21]. Then, the values of $\boldsymbol{v}$ making $h(\boldsymbol{e};\boldsymbol{v})$ a near-optimal IS density can be obtained by setting the gradient of the objective function in Equation (16) to be zero as

$$\sum_{j=1}^{n_s} P\left(S=0 | \boldsymbol{e}_j\right) W\left(\boldsymbol{e}_j ; \boldsymbol{w}\right) \nabla_{\boldsymbol{v}} \ln h\left(\boldsymbol{e}_j ; \boldsymbol{v}\right)=0. \tag{17}$$

4.2.3 | Proposed Adaptive Importance Sampling of RB Particles for Large-Scale Systems

Various studies on CE-AIS [21, 23, 25] have shown that Gaussian mixtures can effectively describe a near-optimal IS density, which has the form of

$$h(\boldsymbol{e} ; \boldsymbol{v})=\sum_{k=1}^{n_{\mathrm{GM}}} \pi_k N\left(\boldsymbol{e} | \boldsymbol{\mu}_k, \boldsymbol{\Sigma}_k\right), \tag{18}$$

where n_{GM} is the number of Gaussian distributions in the mixture; π_k is the probability that the kth Gaussian component is selected, with $\sum_{k=1}^{n_{\mathrm{GM}}} \pi_k = 1$; $N(\boldsymbol{e}|\boldsymbol{\mu}_k,\boldsymbol{\Sigma}_k)$ is the joint PDF of the Gaussian distribution with a mean vector $\boldsymbol{\mu}_k$ and a covariance matrix $\boldsymbol{\Sigma}_k$; and $\boldsymbol{v}=[\pi_1,\boldsymbol{\mu}_1,\boldsymbol{\Sigma}_1,\ldots,\pi_{n_{\mathrm{GM}}},\boldsymbol{\mu}_{n_{\mathrm{GM}}},\boldsymbol{\Sigma}_{n_{\mathrm{GM}}}]$ is given as a parameter vector with $(3\times n_{\mathrm{GM}})$ components. By substituting Equation (18) into Equation (17) and solving it analytically, one can obtain the updating rule for each component as [50]

$$\pi_k=\frac{\sum_{j=1}^{n_{\mathrm{GM}}} P\left(S=0 | \boldsymbol{e}_j\right) W\left(\boldsymbol{e}_j ; \boldsymbol{w}\right) \gamma_{j,k}}{\sum_{j=1}^{n_{\mathrm{GM}}} P\left(S=0 | \boldsymbol{e}_j\right) W\left(\boldsymbol{e}_j ; \boldsymbol{w}\right)}, \tag{19}$$

$$\boldsymbol{\mu}_k=\frac{\sum_{j=1}^{n_{\mathrm{GM}}} P\left(S=0 | \boldsymbol{e}_j\right) W\left(\boldsymbol{e}_j ; \boldsymbol{w}\right) \gamma_{j,k} \boldsymbol{e}_j}{\sum_{j=1}^{n_{\mathrm{GM}}} P\left(S=0 | \boldsymbol{e}_j\right) W\left(\boldsymbol{e}_j ; \boldsymbol{w}\right) \gamma_{j,k}}, \tag{20}$$

$$\boldsymbol{\Sigma}_k=\frac{\sum_{j=1}^{n_{\mathrm{GM}}} P\left(S=0 | \boldsymbol{e}_j\right) W\left(\boldsymbol{e}_j ; \boldsymbol{w}\right) \gamma_{j,k}\left(\boldsymbol{e}_j-\boldsymbol{\mu}_k\right)\left(\boldsymbol{e}_j-\boldsymbol{\mu}_k\right)^{\mathrm{T}}}{\sum_{j=1}^{n_{\mathrm{GM}}} P\left(S=0 | \boldsymbol{e}_j\right) W\left(\boldsymbol{e}_j ; \boldsymbol{w}\right) \gamma_{j,k}}, \tag{21}$$

where $\gamma_{j,k}=\pi_k N(x_j|\boldsymbol{\mu}_k,\boldsymbol{\Sigma}_k)/[\sum_{i=1}^{n_{\mathrm{GM}}} \pi_i N(x_j|\boldsymbol{\mu}_i,\boldsymbol{\Sigma}_i)]$.

However, when CE-AIS is applied to high-dimensional problems, the covariance matrix $\boldsymbol{\Sigma}_k$ computed in Equation (21) may not be positive semidefinite due to numerical errors or limited number of samples [51]. This requires additional steps, such as outlier removal, which becomes more frequent as the dimensionality increases. To prevent this issue, in this paper, all $\boldsymbol{\Sigma}_k$ is set equal to the covariance matrix of $\boldsymbol{e}$, that is, $\boldsymbol{\Sigma}_{\boldsymbol{ee}}$, and only π_k and $\boldsymbol{\mu}_k$ are updated using Equations (19) and (20). Then, the number of components that need to be updated in $\boldsymbol{v}$ becomes $(2\times n_{\mathrm{GM}})$. This approach, called Rao-Blackwellized cross-entropy-based semiadaptive importance sampling (RB-CE-SAIS), has a slower convergence speed compared to the conventional CE-AIS. However, it can eliminate the likely risk of divergence of the covariance matrix. The detailed process of the proposed RB-CE-SAIS is described step by step as follows:

1. *Initialization*: Choose appropriate initial values of parameters $\boldsymbol{v}^0$, that is, π_k^0, $\boldsymbol{\mu}_k^0$, and $\boldsymbol{\Sigma}_k^0$. For example, all π_k^0 are set to be equal (i.e., $\pi_1^0=\pi_2^0=\cdots=\pi_{n_{\mathrm{GM}}}^0=1/n_{\mathrm{GM}}$). For $\boldsymbol{\mu}_k^0$, from the authors' experience, it is recommended to set the mean vector $\boldsymbol{\mu}_k^0$ of the pre-sampling round to $c_k\times[1,1,\ldots,1]$, where c_k is a random scalar value. This results in better convergence compared to randomly setting $\boldsymbol{\mu}_k^0$. Finally, as mentioned above, $\boldsymbol{\Sigma}_k^0$ for all $k\in[1,n_{\mathrm{GM}}]$ is set to $\boldsymbol{\Sigma}_{\boldsymbol{ee}}$. These parameter values are used for both $\boldsymbol{v}$ and $\boldsymbol{w}$.
2. *Sampling*: Generate n_s random samples of total residuals, $\boldsymbol{e}_1,\ldots,\boldsymbol{e}_{n_{\mathrm{GM}}}$, using $h(\boldsymbol{e};\boldsymbol{w})$. To this end, the individual Gaussian densities for sampling $\boldsymbol{e}_j$ are chosen proportional to each π_k. Then, a corresponding number of samples are generated from every Gaussian density.
3. *Convergence check*: Estimate P_f and calculate its coefficient of variation (δ_{P_f}). Note that it is desirable to calculate δ_{P_f} for the full sample as well as when excluding the initial sample set. This is because the initial sample set includes the output where $h(\boldsymbol{e};\boldsymbol{v}^0)$ is far from the optimal IS density. If at least one δ_{P_f} satisfies the convergence requirement (e.g., less than 5%), the algorithm is terminated. Otherwise, proceed to Step 4.
4. *Updating*: Calculate the near-optimal IS density by applying the updating rules in Equations (19) and (20) and return to Step 2.

5 | Numerical Examples

Three numerical examples are presented to demonstrate the proposed algorithm in this section: (1) the example graph in Figure 4, (2) a random graph with two cycles, and (3) the Eastern Massachusetts (EMA) transportation network [52]. All computational analyses were conducted on a personal computer

equipped with an AMD Ryzen 5 3600 3.60 GHz CPU and 16GB of RAM. According to empirical observations, the computer with the given specifications can manage graphs with a maximum clique size of no more than 25 after RB, which covers most lifeline networks except for extreme topologies such as the complete graph. The examples selected for this demonstration all conform to this criterion after sampling the correlated total residuals.

In the examples, a structure (e.g., a bridge) is assumed to be located at the center of each arc and determine the arc's connectivity. The seismic capacity parameters for all structures are homogeneously assumed to be 0.98 for the median $\bar{C}_i$ and 0.69 for the log standard deviation ζ_i. For the prediction of the mean of the seismic demand, denoted by $f(\cdot)$ in Equation (9), and the intraevent spatial correlation, denoted by $\rho_{\varepsilon_i\varepsilon_j}$ in Equation (10), the models proposed in [53] are adopted as follows, respectively.

$$f(M_w, R_i) = -0.5265 - 0.0115\sqrt{R_i^2 + 1.35^2} + \ln\left(R_i^2 + 1.35^2\right)\left[-0.3303 + 0.0599\,(M_w - 4.5)\right], \quad (22)$$

$$\rho_{\varepsilon_i\varepsilon_j}\left(\Delta_{ij}\right) = \exp\left(-0.27\Delta_{ij}^{0.40}\right), \quad (23)$$

where M_w is the moment magnitude; and R_i and Δ_{ij} are given in km. The standard deviations of inter- and intraevent residuals, σ_η and σ_ε, are assumed to 0.265 and 0.502, respectively.

5.1 | Example 1: Example Graph in Figure 4

Consider the example graph in Figure 4, which consists of four vertices and five directional arcs. We consider an earthquake scenario that has a moment magnitude of $M_w = 6.0$ and the epicenter located at distances of 19.09, 23.45, 22.25, 21.47, and 25.43 km from the centers of Arcs 1 through 5, respectively. Before the seismic SRA, the maximum clique size of the graph is given by 4, as shown in Figure 7a. Figure 7b shows that the maximum clique for the seismic SRA (e.g., 10) is exceptionally within the addressable range even without RB in this example, so that the exact system failure probability and parameter sensitivities can be evaluated without sampling.

In this example, since the residual vector is only five-dimensional, that is, $\boldsymbol{e} \in \mathbb{R}^5$, Rao-Blackwellized CE-AIS (RB-CE-AIS), which updates $\boldsymbol{\Sigma}_k$ using Equation (19) as well as π_k and $\boldsymbol{\mu}_k$, can be performed inexpensively. Before comparing the performances of different SRA methods, we first explore the optimal n_{GM} for the RB-CE-AIS and the RB-CE-SAIS. In the presampling round of both methods, c_k is drawn from a uniform distribution $U(0.5, 1)$, and the number of samples generated in each round, n_s, is set to 500. The total number of samples required to achieve a target δ_{P_f} of 1% under varying n_{GM} values is detailed in Appendix A.1. For the continuous objective function $P(S = 0|\boldsymbol{e})$ and the low dimensionality of $\boldsymbol{e}$, employing a single Gaussian (SG), that is, $n_{\mathrm{GM}} = 1$, proves to be more sample-efficient than using GM, according to the results of both CE methods. It is noteworthy that the optimal number of mixtures depends on the specific problem. Especially for problems with multiple failure regions, using an insufficient n_{GM} may fail to fit the optimal IS density in Equation (13) due to the lack of flexibility, thereby resulting in biased failure probability estimates.

Figure 11a shows the failure probabilities with the 95% confidence intervals estimated by RB-CE-AIS with SG, RB-CE-SAIS with SG, the crude RB (RB without IS), and the crude Monte Carlo simulation (MCS), plotted against the number of samples. These estimates are compared to the exact system failure probability obtained without RB, $P_{f,\mathrm{exact}}$ (black dashed line). Each method continues to run until δ_{P_f} of the estimate reaches 1%, with all methods providing almost identical estimates. Figure 11b details the trajectories of δ_{P_f} for each method relative to the number of samples. During the presampling round, δ_{P_f} of two adaptive IS methods are similar, reflecting their shared initialization setting. However, RB-CE-AIS achieves faster convergence than RB-CE-SAIS, as it adaptively optimizes both $\boldsymbol{\Sigma}_k$ and $\boldsymbol{\mu}_k$ to more effectively pinpoint the optimal design point. Despite the faster convergence of RB-CE-AIS, RB-CE-SAIS still significantly outperforms the crude RB or MCS; for the 1% δ_{P_f}, RB and MCS require nearly 316 times and 5,621 times more samples, respectively, than RB-CE-SAIS. Consequently, to achieve the same level of δ_{P_f}, the required number of samples decreases in the order of MCS, RB, RB-CE-SAIS, and RB-CE-AIS, reflecting the varying efficiencies of these methods.

For efficient retrofitting of system components to enhance reliability, we perform probabilistic inference to evaluate the sensitivities of the system failure probability with respect to $\bar{C}_i$ for $i = 1, \ldots, 5$. It is assumed that the variation in $\overline{C_i}$ per unit cost for all homogenous components, $\Delta\bar{C}_i$, is set at 0.02. Table 4 shows the calculated derivations and upgrade worths, suggesting that reinforcing a_1 would be the most effective in improving system reliability. Given the similar failure probabilities of components, the result is driven by the topological properties of the network. For instance, if Arc 1 with the highest $I_{\bar{C}_i}$ fails (i.e., $X_1 = 0$), the OD connectivity totally relies on the path comprising Arcs 2 and 5. Conversely, the failure of Arc 3 with the lowest $I_{\bar{C}_i}$ (i.e., $X_3 = 0$) less critically affects the system, since there still remain two separate alternative paths between the OD pair: via Arcs 1 and 4, as well as Arcs 2 and 5.

5.2 | Example 2: Cyclic Random Graph

Figure 12 shows a cyclic random graph with 12 vertices and 20 directional arcs that includes two cycles—a triangular one and a square one (i.e., $n_{\mathrm{cyc}} = 2$, $n_1 = 3$, and $n_2 = 4$). The red concentric circles indicate the location of the epicenter, and the earthquake scenario has a moment magnitude $M_w = 4.5$. The cyclic graph can be decomposed into 20 directed acyclic subgraphs, each having a maximum clique size of 8. By utilizing the proposed method, the failure probability for each acyclic subgraph is calculated, and the results are integrated using Equation (3) to estimate the overall failure probability of the original graph. Given the high dimensionality of the residual vector in this case, the update process for $\boldsymbol{\Sigma}_k$ in RB-CE-AIS becomes computationally burdensome and often results in matrices that are not positive semidefinite. Consequently, RB-CE-SAIS is exclusively used to determine the required number of samples to achieve $\delta_{P_f} = 1\%$, as outlined in Appendix A.2. Based on the results, $n_{\mathrm{GM}} = 2$ is selected, which is also used to assess the performance of RB-CE-AIS.

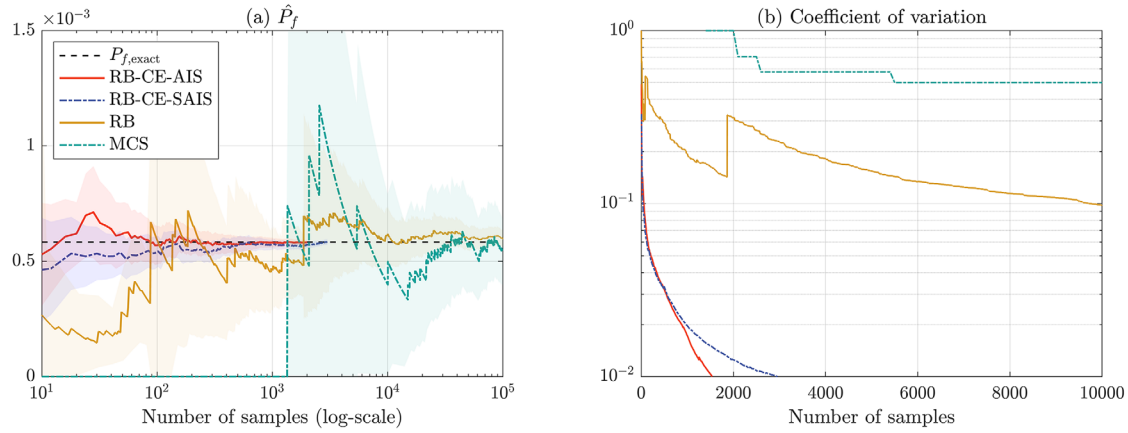

FIGURE 11 | (a) Estimated failure probabilities of the graph in Figure 4; and (b) the coefficient of variation δ_{P_f}.

TABLE 4 | Results of sensitivity analysis of example graph.

i	1	2	3	4	5
$\frac{\partial P_f}{\partial \bar{C}_i}$	-9.99×10^{-4}	-6.40×10^{-4}	-3.07×10^{-5}	-4.15×10^{-4}	-9.15×10^{-4}
$I_{\bar{C}_i}$	2.00×10^{-5}	1.28×10^{-5}	6.14×10^{-7}	8.31×10^{-6}	1.83×10^{-5}

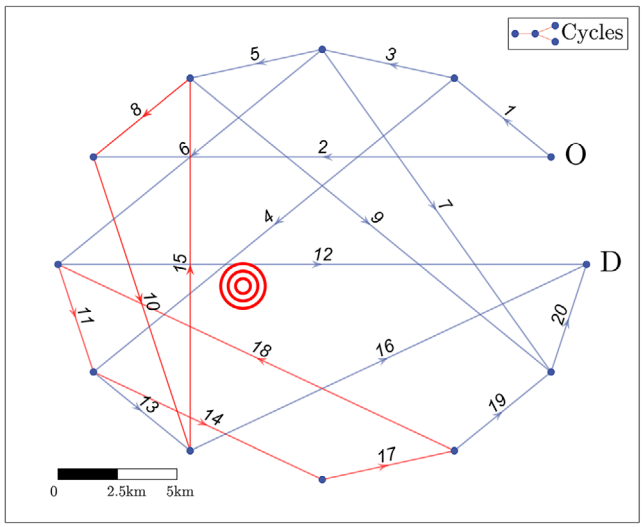

FIGURE 12 | Random directed graph with two cycles.

Figure 13 compares the results of seismic SRA and δ_{P_f}. In Figure 13a, RB-CE-AIS initially produces a close match to the proposed method in the early phase of analysis. However, Figure 13b shows that the convergence rate of RB-CE-AIS is significantly lower than that of RB-CE-SAIS after the first update of $\boldsymbol{\Sigma}_k$. Notably, beyond 3,000 samples, δ_{P_f} sharply increases, and further sample generation becomes problematic when the sample count exceeds about 7,000 due to the failure of $\boldsymbol{\Sigma}_k$ to remain positive semidefinite. By contrast, the proposed method demonstrates the efficiency and stable convergence toward $\delta_{P_f} = 1\%$ with only about 4,000 samples. This performance is substantially more efficient than those of RB and MCS, which require approximately 729,000 and 6.83 million samples, respectively, to achieve similar levels of precision.

Then, the parameter sensitivity and the upgrade worth are calculated to assess the importance of each component. In this example, the values of $\Delta\bar{C}_i$ by unit price are set to be inversely proportional to the length of each arc (in km). The results from this parameter sensitivity analysis are detailed in Table 5. Arcs 1, 3, and 20, near Vertices O or D, are identified as the components that yield the most significant improvement in system reliability per unit reinforcement cost invested. Such insights are crucial for prioritizing investment in the upgrade of lifeline systems, ensuring that limited resources are allocated in a manner that maximizes the return in terms of enhanced reliability and reduced vulnerability.

5.3 | Example 3: EMA Transportation Network

Figure 14a shows a preplanned lane reversal scenario of the EMA transportation network, comprising 129 unidirectional arcs and 74 vertices. The origin and destination are specified as the south and north-east of Boston, respectively. We consider an earthquake scenario with a moment magnitude $M_w = 6.0$. The coordinates of the epicenter are given as 42°24′ N and 70°54′ W, respectively. Since some arcs are independent of the OD connectivity, the network can be simplified as shown in Figure 14b by eliminating them. The simplification process reduces the number of directional arcs and vertices to 85 and 47, respectively. The maximum clique size, a key factor influencing computational complexity, remains constant at sixteen, suggesting that both are computationally manageable with a computer configuration of 16GB of RAM. Although the simplification does not drastically alter computational complexity (e.g., *COL* only decreases from 112,344 to 78,208), it provides significant computational advantages in performing sensitivity analysis in that the number of target parameters has been reduced from 129 to 85.

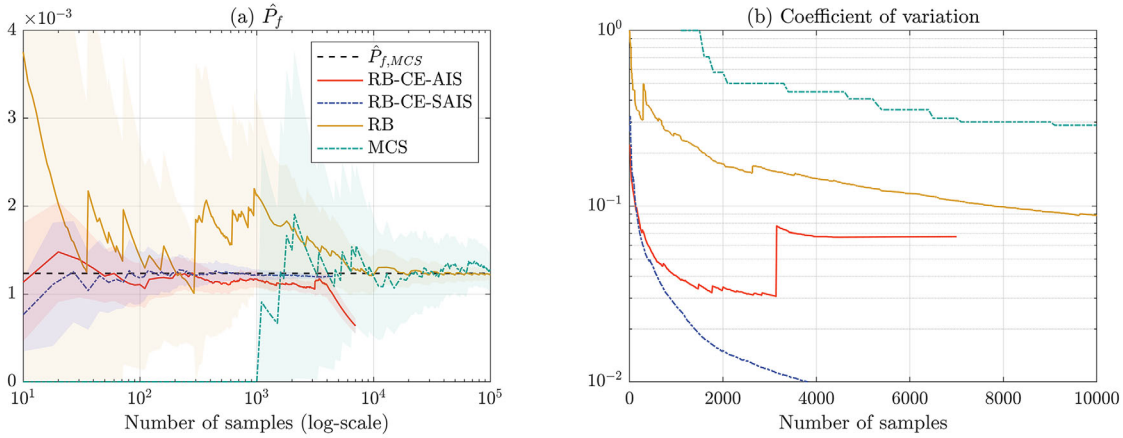

FIGURE 13 | (a) Estimated failure probabilities of the cyclic random graph; and (b) the coefficient of variation δ_{P_f}.

TABLE 5 | Parameters and results of sensitivity analysis of the cyclic random graph.

i	1	2	3	4	5	6	7
$\Delta\bar{C}_i$	0.174	0.0519	0.174	0.0466	0.174	0.0636	0.0519
$\frac{\partial P_f}{\partial \bar{C}_i}$	-2.18×10^{-3}	-6.04×10^{-4}	-7.74×10^{-4}	-4.01×10^{-4}	-2.56×10^{-5}	-9.11×10^{-5}	-8.90×10^{-5}
$I_{\bar{C}_i}$	3.78×10^{-4}	3.14×10^{-5}	1.34×10^{-4}	1.86×10^{-5}	4.45×10^{-6}	5.79×10^{-6}	4.62×10^{-6}
i	8	9	10	11	12	13	14
$\Delta\bar{C}_i$	0.174	0.0466	0.0636	0.174	0.0450	0.174	0.0899
$\frac{\partial P_f}{\partial \bar{C}_i}$	-1.69×10^{-6}	-1.18×10^{-4}	-1.03×10^{-3}	-4.37×10^{-5}	-1.44×10^{-4}	-7.96×10^{-5}	-6.80×10^{-5}
$I_{\bar{C}_i}$	2.94×10^{-7}	5.51×10^{-6}	6.53×10^{-5}	7.60×10^{-6}	6.47×10^{-6}	1.38×10^{-5}	6.12×10^{-6}
i	15	16	17	18	19	20	
$\Delta\bar{C}_i$	0.0519	0.0519	0.174	0.0519	0.174	0.174	
$\frac{\partial P_f}{\partial \bar{C}_i}$	-3.70×10^{-5}	-2.23×10^{-4}	-2.46×10^{-5}	-1.06×10^{-5}	-3.94×10^{-5}	-2.57×10^{-4}	
$I_{\bar{C}_i}$	1.92×10^{-6}	1.16×10^{-5}	4.27×10^{-6}	5.51×10^{-7}	6.85×10^{-6}	4.46×10^{-5}	

TABLE 6 | Estimated failure probability and number of samples required for $\delta_{P_f} = 1\%$ (without correlations).

Network types	**Original**		**Simplified**	
Methods	**Proposed method**	**MCS**	**Proposed method**	**MCS**
$\hat{P}_f$ ($\times10^{-5}$)	1.652	1.667	1.652	1.660
Number of samples	—	5.92×10^{8}	—	5.98×10^{8}
Computational time (s)	1.83	1.86×10^{4}	1.21	1.73×10^{4}

If component failure events are assumed to be statistically independent (i.e., if the correlations between the total residuals of seismic demands are ignored), the exact system failure probability can be evaluated directly by the message-passing of the JT as mentioned in Section 3.3.2. Table 6 presents the evaluated system failure probability and the computational costs of the proposed method with and without graph simplification, in comparison to the results of MCS. The results confirm that simplification only impacts the computational time of the proposed BN-based method, while the exact failure probability remains constant. It is noteworthy that while the proposed method evaluates the exact system failure probability, the computational time is significantly shorter than that required by MCS in both cases.

Conversely, when the correlations are not ignored, RB-CE-SAIS with SG (i.e., $n_{\mathrm{GM}} = 1$) consistently delivers the best performance in both the original and simplified network configurations (see details in Appendix A.3). Table 7 presents a summary of the results from each method, focusing on the failure probability estimates and the number of samples required to achieve $\delta_{P_f} = 1\%$.

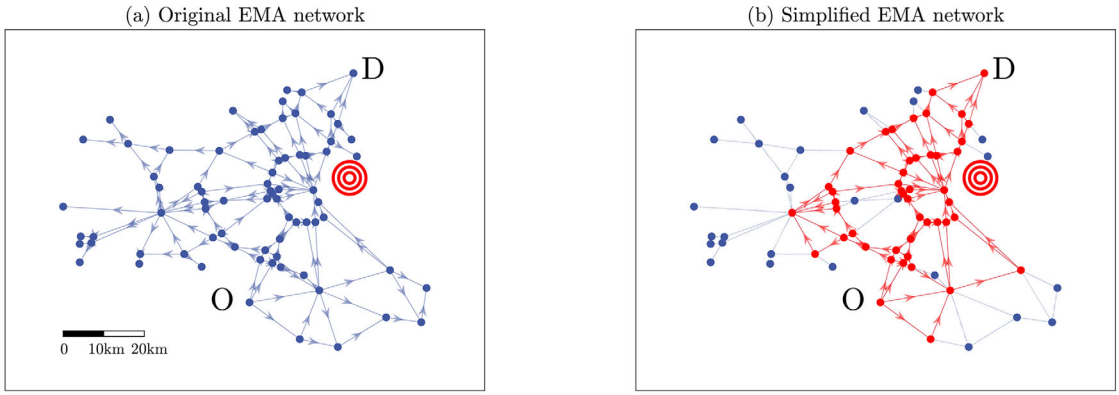

FIGURE 14 | (a) Eastern Massachusetts (EMA) highway network; and (b) simplified one.

TABLE 7 | Estimated failure probability and number of samples required for $\delta_{P_f} = 1\%$ (with correlations).

Network types	Original			Simplified		
Methods	**RB-CE-SAIS**	**RB**	**MCS**	**RB-CE-SAIS**	**RB**	**MCS**
$\hat{P}_f$ ($\times 10^{-4}$)	1.476	1.486	1.477	1.491	1.451	1.480
Number of samples	1.54×10^4	1.90×10^6	6.77×10^7	8.91×10^3	1.94×10^6	6.76×10^7

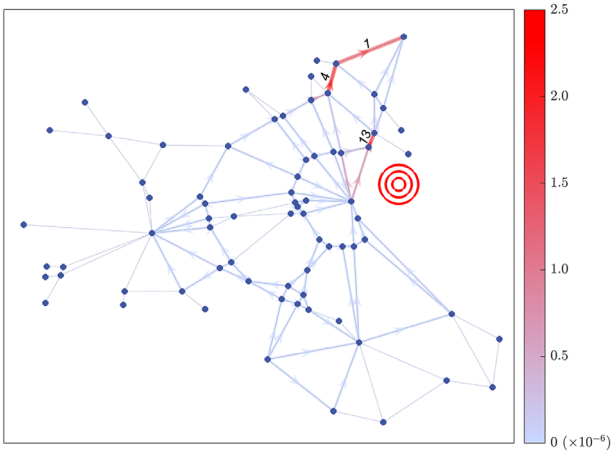

FIGURE 15 | Eastern Massachusetts (EMA) network highlighting the upgrade worth of each arc.

Across both network configurations, RB-CE-SAIS demonstrates significantly superior sample efficiency when compared to the crude RB and MCS. Moreover, it is noteworthy that graph simplification has no impact on the sample efficiency of RB or MCS, which is only contingent on the target probability. Conversely, the proposed RB-CE-SAIS method benefits markedly from the graph simplification. The decreased dimensionality from $\boldsymbol{e} \in \mathbb{R}^{129}$ to $\boldsymbol{e} \in \mathbb{R}^{85}$ boosts a more efficient identification of near-optimal IS PDFs, in turn enhancing the sample efficiency of RB-CE-SAIS.

In the sensitivity analysis of the simplified network, the values of $\Delta\bar{C}_i$ by unit price for each arc are assumed to be identical to 0.01. This assumption simplifies the comparison of each upgrade worth by focusing solely on the derivatives $\partial P_f / \partial \bar{C}_i$. The analysis results are illustrated in Figure 15, in which the arcs with the highest upgrade worth are prominently highlighted in red. From a topological perspective, Arcs 1 and 4 are located near the vertex D, and the surrounding arcs converge toward them. This makes these arcs highly sensitive to the system failure probability with respect to $\bar{C}_i$, despite their relative distance from the seismic epicenter. Meanwhile, the high sensitivity of Arc 13 can be primarily attributed to its geographical placement closer to the epicenter, making it prone to fail.

6 | Conclusions

This paper introduces a novel BN-based method for SRA of the connectivity of directed graphs, which employs the JT algorithm and dual graph representation. The integration of graph theory and BN approach enables a systematic automation of BN modeling for SRA, thereby evaluating the system failure probability analytically especially when component events are statistically independent. To extend the proposed framework to a large-scale network with dependent component events, represented by seismic hazards, this study proposes incorporating IS and RB into the proposed method. In addition, we demonstrate how sensitivity analysis can be performed by the proposed framework and propose several preprocessing procedures to relax constraints on the addressable systems.

The proposed method offers three key advantages: (1) the method can be implemented by existing BN algorithms available in general-purpose software programs; (2) a useful metric is provided to quantify the complexity of a network system from the perspective of SRA; and (3) SRA of large-scale network systems can be efficiently performed to evaluate system failure probability or parameter sensitivity. Three numerical examples under seismic scenarios highlight the accuracy and efficiency of the proposed method compared to existing methods.

The BN-based framework proposed in this paper is highly extensible, and in particular, the computational complexity quantification and probabilistic inference (including sensitivity analysis) methods can be applied to other fields, including structural reliability and earthquake engineering. In future work, additional sampling may be introduced to promote wide application of the proposed method to local road networks in dense areas as well as highway lane reversal scenarios and to mitigate the computational complexity of maximum cliques, which is the bottleneck of SRA in the proposed framework. Potential extensions of the research topic include (1) analyzing the connectivity of multiple OD pairs, and (2) developing the proposed approach for maximum flow analysis or average travel time with multistate components beyond system connectivity for a comprehensive understanding of network performance.

Acknowledgments

This work is supported by the National Research Foundation of Korea (NRF) grant funded by the Korea government (MSIT) (RS-2021-NR059025). The first author is also supported by the Basic Science Research Program through the NRF grant funded by the Ministry of Education (RS-2024–00408907). The third author is also supported by the Institute of Construction and Environmental Engineering at Seoul National University.

Conflicts of Interest

The authors declare no conflicts of interest.

Data Availability Statement

The data that support the findings of this study are available from the corresponding author upon reasonable request.

References

1. B. M. Williams, A. P. Tagliaferri, S. S. Meinhold, J. E. Hummer, and N. M. Rouphail, "Simulation and Analysis of Freeway Lane Reversal for Coastal Hurricane Evacuation," *Journal of Urban Planning and Development* 133, no. 1 (2007): 61–72.

2. T. Li, N. Wang, M. Zhang, and Z. He, "Dynamic Reversible Lane Optimization in Autonomous Driving Environments: Balancing Efficiency and Safety," *Journal of Industrial and Management Optimization* 20, no. 3 (2024): 901–925.

3. M. Hohenbichler and R. Rackwitz, "First-Order Concepts in System Reliability," *Structural Safety* 1, no. 3 (1982): 177–188.

4. J. Song and A. Der Kiureghian, "Bounds on System Reliability by Linear Programming," *Journal of Engineering Mechanics* 129, no. 6 (2003): 627–636.

5. Y. Chang and Y. Mori, "A Study on the Relaxed Linear Programming Bounds Method for System Reliability," *Structural Safety* 41 (2013): 64–72.

6. D. Lee and J. Song, "Multi-Scale Seismic Reliability Assessment of Networks by Centrality-Based Selective Recursive Decomposition Algorithm," *Earthquake Engineering & Structural Dynamics* 50, no. 8 (2021): 2174–2194.

7. G. S. Fishman, "A Monte Carlo Sampling Plan for Estimating Network Reliability," *Operations Research* 34, no. 4 (1986): 581–594.

8. K. M. Zuev, S. Wu, and J. L. Beck, "General Network Reliability Problem and Its Efficient Solution by Subset Simulation," *Probabilistic Engineering Mechanics* 40 (2015): 25–35.

9. X. Liu, S. Zheng, X. Wu, D. Chen, and J. He, "Research on a Seismic Connectivity Reliability Model of Power Systems Based on the Quasi-Monte Carlo Method," *Reliability Engineering & System Safety* 215 (2021): 107888.

10. D. Lee, Z. Wang, and J. Song, "Efficient Seismic Reliability and Fragility Analysis of Lifeline Networks Using Subset Simulation," *Reliability Engineering & System Safety* 260 (2025): 110947.

11. C. M. Rocco and J. A. Moreno, "Fast Monte Carlo Reliability Evaluation Using Support Vector Machine," *Reliability Engineering & System Safety* 76, no. 3 (2002): 237–243.

12. M. A. Nabian and H. Meidani, "Deep Learning for Accelerated Seismic Reliability Analysis of Transportation Networks," *Computer-Aided Civil and Infrastructure Engineering* 33, no. 6 (2018): 443–458.

13. J. Pearl, *Probabilistic Reasoning in Intelligent Systems: Networks of Plausible Inference* (Morgan Kaufmann, 1988).

14. M. Bensi, A. Der Kiureghian, and D. Straub, "Efficient Bayesian Network Modeling of Systems," *Reliability Engineering & System Safety* 112 (2013): 200–213.

15. I. Tien and A. Der Kiureghian, "Algorithms for Bayesian Network Modeling and Reliability Assessment of Infrastructure Systems," *Reliability Engineering & System Safety* 156 (2016): 134–147.

16. J. E. Byun, K. Zwirglmaier, D. Straub, and J. Song, "Matrix-Based Bayesian Network for Efficient Memory Storage and Flexible Inference," *Reliability Engineering & Systems Safety* 185 (2019): 533–545.

17. J. E. Byun and J. Song, "A General Framework of Bayesian Network for System Reliability Analysis Using Junction Tree," *Reliability Engineering & System Safety* 216 (2021): 107952.

18. P. Gehl, R. Fayjaloun, L. Sun, et al., "Rapid Earthquake Loss Updating of Spatially Distributed Systems via Sampling-Based Bayesian Inference," *Bulletin of Earthquake Engineering* 20, no. 8 (2022): 3995–4023.

19. K. Zwirglmaier, J. Chan, I. Papaioannou, J. Song, and D. Straub, "Hybrid Bayesian Networks for Reliability Assessment of Infrastructure Systems," *ASCE-ASME Journal of Risk and Uncertainty in Engineering Systems, Part A: Civil Engineering* 10, no. 2 (2024): 04024019.

20. M. Bensi, A. Der Kiureghian, and D. Straub, A Bayesian Network Methodology for Infrastructure Seismic Risk Assessment and Decision Support, PEER Report 2011/02 (Pacific Earthquake Engineering Research Center, 2011), https://apps.peer.berkeley.edu/publications/peer_reports/reports_2011/webPEER-2011-02-BENSIetal.pdf.

21. N. Kurtz and J. Song, "Cross-Entropy-Based Adaptive Importance Sampling Using Gaussian Mixture," *Structural Safety* 42 (2013): 35–44.

22. Z. Wang and J. Song, "Cross-Entropy-Based Adaptive Importance Sampling Using von Mises-Fisher Mixture for High Dimensional Reliability Analysis," *Structural Safety* 59 (2016): 42–52.

23. D. Y. Yang, J. G. Teng, and D. M. Frangopol, "Cross-Entropy-Based Adaptive Importance Sampling for Time-Dependent Reliability Analysis of Deteriorating Structures," *Structural Safety* 66 (2017): 38–50.

24. B. S. Choi and J. Song, "Cross-Entropy-Based Adaptive Importance Sampling for Probabilistic Seismic Risk Assessment of Lifeline Networks Considering Spatial Correlation," *Procedia Engineering* 198 (2017): 999–1006.

25. S. Geyer, I. Papaioannou, and D. Straub, "Cross Entropy-Based Importance Sampling Using Gaussian Densities Revisited," *Structural Safety* 76 (2019): 15–27.

26. O. Kanjilal, I. Papaioannou, and D. Straub, "Cross Entropy-Based Importance Sampling for First-Passage Probability Estimation of Randomly Excited Linear Structures With Parameter Uncertainty," *Structural Safety* 91 (2021): 102090.

27. D. Koller and N. Friedman, *Probabilistic Graphical Models: Principles and Techniques* (MIT Press, 2009).

28. D. J. Spiegelhalter, A. P. Dawid, S. L. Lauritzen, and R. G. Cowell, "Bayesian Analysis in Expert Systems," *Statistical Science* 8, no. 3 (1993): 219–247.

29. D. Barber, *Bayesian Reasoning and Machine Learning* (Cambridge University Press, 2012).

30. M. O. Ball, "Computational Complexity of Network Reliability Analysis: An Overview," *IEEE Transactions on Reliability* 35, no. 3 (1986): 230–239.

31. C. J. Colbourn, "Network Resilience," *SIAM Journal on Algebraic Discrete Methods* 8, no. 3 (1987): 404–409.

32. M. O. Ball, C. J. Colbourn, and J. S. Provan, "Network Reliability," *Handbooks in Operations Research and Management Science* 7 (1995): 673–762.

33. S. Porta, P. Crucitti, and V. Latora, "The Network Analysis of Urban Streets: A Dual Approach," *Physica A: Statistical Mechanics and Its Applications* 369, no. 2 (2006): 853–866.

34. H. W. Lim and J. Song, "Efficient Risk Assessment of Lifeline Networks Under Spatially Correlated Ground Motions Using Selective Recursive Decomposition Algorithm," *Earthquake Engineering & Structural Dynamics* 41, no. 13 (2012): 1861–1882.

35. D. Lee, J. E. Byun, J. Song, and K. Sadeghi, "Network Reliability Analysis and Complexity Quantification Using Bayesian Network and Dual Representation," in *Proceedings of the 14th International Conference on Applications of Statistics and Probability in Civil Engineering (ICASP14)* (Trinity College Dublin, 2023).

36. F. V. Jensen and F. Jensen, "Optimal Junction Trees," in *Proceedings of the Tenth Conference on Uncertainty in Artificial Intelligence*, 1994 (1994), 360–366, https://arxiv.org/abs/1302.6823.

37. L. G. Valiant, "The Complexity of Enumeration and Reliability Problems," *SIAM Journal on Computing* 8, no. 3 (1979): 410–421.

38. H. Chan and A. Darwiche, "Sensitivity Analysis in Bayesian Networks: From Single to Multiple Parameters," *arXiv preprint arXiv:1207.4124* (2012).

39. A. Der Kiureghian, O. D. Ditlevsen, and J. Song, "Availability, Reliability and Downtime of Systems With Repairable Components," *Reliability Engineering & System Safety* 92, no. 2 (2007): 231–242.

40. J. Song and W. H. Kang, "System Reliability and Sensitivity Under Statistical Dependence by Matrix-Based System Reliability Method," *Structural Safety* 31, no. 2 (2009): 148–156.

41. A. Der Kiureghian, *Structural and System Reliability* (Cambridge University Press, 2022).

42. A. K. Chopra, *Dynamics of Structures: Theory and Applications to Earthquake Engineering* (Prentice-Hall, 1995).

43. J. W. Baker and C. A. Cornell, "A Vector-Valued Ground Motion Intensity Measure Consisting of Spectral Acceleration and Epsilon," *Earthquake Engineering & Structural Dynamics* 34, no. 10 (2005): 1193–1217.

44. N. Luco and C. A. Cornell, "Structure-Specific Scalar Intensity Measures for Near-Source and Ordinary Earthquake Ground Motions," *Earthquake Spectra* 23, no. 2 (2007): 357–392.

45. N. A. Abrahamson and R. R. Youngs, "A Stable Algorithm for Regression Analyses Using the Random Effects Model," *Bulletin of the Seismological Society of America* 82, no. 1 (1992): 505–510.

46. W. B. Joyner and D. M. Boore, "Methods for Regression Analysis of Strong-Motion Data," *Bulletin of the Seismological Society of America* 83, no. 2 (1993): 469–487.

47. B. A. Bradley, "Site-specific and spatially-distributed ground-motion intensity estimation in the 2010-2011 Canterbury earthquakes," *Soil Dynamics and Earthquake Engineering* 61 (2014): 83–91.

48. J. E. Padgett and R. DesRoches, "Sensitivity of Seismic Response and Fragility to Parameter Uncertainty," *Journal of Structural Engineering* 133, no. 12 (2007): 1710–1718.

49. R. Y. Rubinstein and D. P. Kroese, *Simulation and the Monte Carlo Method* (John Wiley & Sons, 2017).

50. R. Y. Rubinstein and D. P. Kroese, *The Cross-Entropy Method: A Unified Approach to Combinatorial Optimization, Monte-Carlo Simulation, and Machine Learning* (Springer, 2004).

51. G. A. Holton, *Value-at-Risk: Theory and Practice* (Academic Press, 2003).

52. J. Zhang, S. Pourazarm, C. G. Cassandras, and I. C. Paschalidis, "The Price of Anarchy in Transportation Networks: Data-Driven Evaluation and Reduction Strategies," *Proceedings of the IEEE* 106, no. 4 (2018): 538–553.

53. D. M. Boore and G. M. Atkinson, "Ground-Motion Prediction Equations for the Average Horizontal Component of PGA, PGV, and 5%-Damped PSA at Spectral Periods Between 0.01 s and 10.0 s," *Earthquake Spectra* 24, no. 1 (2008): 99–138.

Appendix A: Detailed Results of Numerical Examples in Section 5

TABLE A.1 | Number of samples required to achieve $\delta_{P_f} = 1\%$ in Example 1.

Number of Gaussian mixtures, n_{GM}	RB-CE-AIS	RB-CE-SAIS
1	1,595	2,985
2	1,954	3,718
5	2,196	3,866
10	2,179	3,324
50	2,259	3,370
100	2,269	3,122

TABLE A.2 | Number of samples required to achieve $\delta_{P_f} = 1\%$ in Example 2.

Number of Gaussian mixtures, n_{GM}	RB-CE-SAIS
1	3,970
2	3,728
5	4,158
10	3,993
50	3,860
100	4,032

TABLE A.3 | Number of samples required to achieve $\delta_{P_f} = 1\%$ for the original and simplified EMA networks.

Number of Gaussian mixtures, n_{GM}	Original network	Simplified network
1	15,407	8,907
2	24,673	12,483
5	21,110	9,195
10	16,674	10,250
50	19,020	11,167
100	42,090	11,309